Inorganic Chemistry

Article

pubs.acs.org/IC

New Metal Phthalocyanines/Metal Simple Hydroxide Multilayers: Experimental Evidence of Dipolar Field-Driven Magnetic Behavior

Riadh Bourzami,[†,‡] Séraphin Eyele-Mezui,[†] Emilie Delahaye,[†,§] Marc Drillon,[†,§] Pierre Rabu,[†,§] Nathalie Parizel,*[,‡,§] Sylvie Choua,[‡,§] Philippe Turek,[‡,§] and Guillaume Rogez*[,†,§]

[†]Institut de Physique et Chimie des Matériaux de Strasbourg, UMR 7504 CNRS—Université de Strasbourg, and Labex NIE, 23 rue du Loess, BP 43, 67034 Strasbourg cedex 2, France

[‡]Institut de Chimie, UMR 7177 CNRS—Université de Strasbourg, 1 rue Blaise Pascal, BP 296 R8, 67008 Strasbourg cedex, France

[§]Fondation icFRC International Center for Frontier Research in Chemistry, 8, allée Gaspard Monge F-67000 Strasbourg, France

Supporting Information

ABSTRACT: A series of new hybrid multilayers has been synthesized by insertion-grafting of transition metal (Cu^{II}, Co^{II}, Ni^{II}, and Zn^{II}) tetrasulfonato phthalocyanines between layers of Cu^{II} and Co^{II} simple hydroxides. The structural and spectroscopic investigations confirm the formation of new layered hybrid materials in which the phthalocyanines act as pillars between the inorganic layers. The magnetic investigations show that all copper hydroxide-based compounds behave similarly, presenting an overall antiferromagnetic behavior with no ordering down to 1.8 K. On the contrary, the cobalt hydroxide-based compounds present a ferrimagnetic ordering around 6 K, regardless of the nature of the metal phthalocyanine between the inorganic layers. The latter observation points to strictly dipolar interactions between the inorganic layers. The amplitude of the dipolar field has been evaluated from X-band and Q-band EPR spectroscopy investigation ($B_{dipolar} \approx 30$ mT).

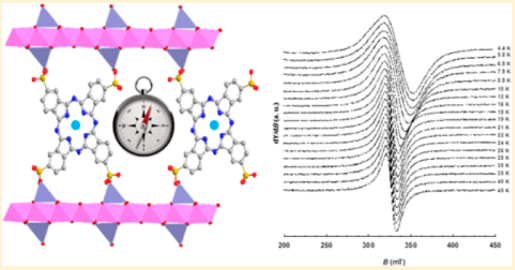

INTRODUCTION

Hybrid organic−inorganic materials can be described as made of two subnetworks, one inorganic and one organic, intimately connected together. They constitute a class of materials of considerable interest.[1−3] The controlled assembly of the two components at a nanoscale level is suitable to provide new multifunctional systems in which each subnetwork exhibits its own properties or contributes synergistically to new physical phenomena and novel applications.[4,5] Layered insertion compounds, in which the properties of each subnetwork and their synergy can be tuned by the topology and chemical bonding between constituents, are particularly worthy of interest.[6] Many works about multifunctional hybrids have investigated layered bimetallic trioxalatometalates,[7,8] hexathiohypodiphosphates (MPS_3),[9] or magnetic layered double hydroxides (LDH),[10] owing to their ability to be functionalized with various ligands via versatile reactions. Very recently, striking results were obtained with respect to the combination of magnetism with chirality,[5] ferroelectricity,[11] superconductivity,[10] or nonlinear optics.[12]

In this field, it is essential to identify and control the structural features and physical mechanisms influencing the properties of these new hierarchically organized nanostructures.[13] The interfaces play a key role here. As an alternative to the previously mentioned layered magnetic materials (class I materials, in which the bonds between the subnetworks are weak[14]), we have focused on the insertion and grafting (strong bond) of functional molecules into magnetic layered simple hydroxides (LSH), with general formulation $M_x(OH)_{2x-ny}(X^{n-})_y$ (M(II) = Co, Cu, Ni, Mn, and X^{n-} = carboxylate, sulfate, or sulfonate anion).[15−17] The X^{n-} anion located in the interlayer space may be substituted by a large variety of molecules via anionic exchange reaction.

The insertion of transition metal complexes into lamellar hosts such as layered oxalates, zirconium phosphate, MPS_3, LDH, or clays or their insertion-grafting into LSH is a very promising route to promote multiple properties such as luminescence,[18−22] chirality,[23,24] or magnetism (additional paramagnetism,[25,26] spin crossover[27−29]) with the advantage of immobilizing the metal complexes in inorganic host structures. In addition these functionalities can be quite easily tuned by changing the metal center.[30]

Among transition metal complexes, the phthalocyanine complexes are worthy of interest. Phthalocyanines have been studied for many years because of their intriguing properties, resulting from their peculiar aromatic electronic structure,[31−33] and they have been particularly used in the field of catalysis,[34−36] organic photovoltaics,[37] organic semiconductors,[38−40] or photodynamic therapy,[41,42] for instance. To improve their properties, to reinforce their stability, or to enable their practical applications, phthalocyanine complexes are often embedded into host materials, such as polymers,[43]

Received: November 5, 2013
Published: January 8, 2014

   dx.doi.org/10.1021/ic4027688 | Inorg. Chem. 2014, 53, 1184−1194

zeolites,[44−47] clays,[44,48−51] or layered double hydroxides.[25,48,52−57]

Apart from one single example,[58] the insertion of phthalocyanine complexes into layered simple hydroxides has never been reported. Actually, the insertion of large molecules into LSH is still a chemical challenge. This is likely due to the cohesion forces between the inorganic layers in the case of LSH, which are more important than in the case of LDH, for example. This difference is further illustrated by the fact that LDH can be exfoliated more easily[59,60] than LSH.[61,62] Actually, whereas interleaved species in LDH are held by coulombic interactions, in LSH, they must be grafted onto the inorganic layers via anchoring groups coordinating the metal cations of the inorganic sheets.

The motivation for the present work stems from different aspects. First, due to the variety of layered hosts encountered in the literature, one needs to advance toward a more comprehensive understanding of interfaces to control the properties of the various hybrid systems obtained. We specially explore the less investigated LSH systems. In these systems, the interaction between the molecular and inorganic components via iono-covalent coordination is quite strong. Moreover, this interaction is a priori tunable by using different coordination functions.

Thus, in this paper, we particularly investigate the possible interplay between the magnetic properties of the LSH hosts and the ones of phthalocyanine guests. We describe the synthesis, structural characterization, and properties of homologous series of new hydroxide-based compounds functionalized by metal−phthalocyanine complexes, with general formulation $M_2(OH)_{4-4x}(M'PcTS_0)_x{\cdot}zH_2O$ (M = Cu, Co, and Zn and M′ = Cu, Co, Ni, and Zn). In the following sections, the hybrid compounds will be referred to as $M'PcTS_0{\subset}M$. Moreover, magnetic measurements coupled to X and Q-band EPR spectroscopy allow an explicit description of the mechanism responsible for the magnetic ordering in layered simple hydroxides.[63]

EXPERIMENTAL SECTION

$Co_2(OH)_3(OAc){\cdot}H_2O$,[64−66] $Cu_2(OH)_3(DS)$[67] and $Zn_5(OH)_8(DS)_2$[68] were prepared as previously described. (NaDS and $NaDS_0$ are sodium dodecylsulfate and dodecylsulfonate, respectively.) All experiments were conducted under argon, and the solvents were degassed prior to use. Yields of the synthesis of hybrid compounds are around 60−70%.

Co(II), Ni(II), and Zn(II) phthalocyanine-4,4′,4″,4‴-tetrasulfonic-acid, tetrasodium salt (**$CoPcTS_0Na_4$**, **$NiPcTS_0Na_4$**, and **$ZnPcTS_0Na_4$**) were synthesized according to published procedures.[69] Cu(II) phthalocyanine-3,4′,4″,4‴-tetrasulfonic-acid, tetrasodium salt (Aldrich, 85%) (**$CuPcTS_0Na_4$**) was used without further purification.

Elemental analyses for C, H, N, S, Co, Cu, and Zn were carried out at the Service Central d'Analyse of the CNRS (USR-59). The powder XRD patterns were collected with a Bruker D8 diffractometer (Cu $K\alpha_1$ = 0.1540598 nm) equipped with a SolX detector discriminating in energy. The SEM images were obtained with a JEOL 6700F (scanning electron microscope (SEM) equipped with a field emission gun, operating at 3 kV in the SEI mode). FT-IR spectra were collected on a Digilab FTS 3000 computer-driven instrument (0.1 mm thick powder samples in KBr). UV/vis/NIR studies were performed on a Perkin-Elmer Lambda 950 spectrometer (spectra recorded in the reflection mode, using a 150 mm integrating sphere, with a mean resolution of 2 nm and a sampling rate of 300 nm·min^{-1}). TGA-TDA experiments were performed using a Setaram TG92 instrument (heating rate of 5 °C·min^{-1}, air stream). The magnetic studies were carried out with a SQUID magnetometer (Quantum Design MPMS-XL) covering the temperature and fields ranges of 2−300 K, ± 5 T. The ac susceptibility measurements were performed in a 0.35 mT alternative field (100 Hz). Magnetization measurements at different fields at room temperature confirm the absence of ferromagnetic impurities. X-band EPR spectra were recorded with a continuous-wave ESP-300-E spectrometer (Bruker Biospin GmbH, Germany). The resonator is a Bruker ER 4102ST standard rectangular cavity operating in the TE_{108} mode equipped with an ESR900 Oxford cryostat (ν∼9.3 GHz in X-band, and ν∼34 GHz in Q-band). Temperature was measured within the 4−300 K temperature range with a Cernox sensor (accuracy: $\Delta T/T \sim 5\%$). The spectrometer was tuned so as the settings (modulation coils, incident microwave power) do not distort the EPR signal. Simulations were generated with the EasySpin free software.[70]

$CuPcTS_0{\subset}Cu$ (1). **$CuPcTS_0Na_4$** (453 mg, 0.46 mmol) was dissolved in 30 mL of water, and the pH was adjusted to 8 using HCl 0.2 M. At this stage, $Cu_2(OH)_3(DS)$ (260 mg, 0.59 mmol) was added along with 20 mL of ethanol, and the mixture was stirred for 8 h at 80 °C under argon. The blue powder was collected after four centrifugations (8000 rpm, 10 min each), and the supernatant was replaced after each centrifugation by distilled water in order to wash the product. The collected solid was finally washed with ethanol and dried under vacuum.

Anal. Calcd for $Cu_2(OH)_{3.12}(CuPcTS_0)_{0.22}{\cdot}3H_2O$, $Cu_{2.22}C_{7.04}H_{5.76}N_{1.76}S_{0.88}O_{5.76}{\cdot}3.0H_2O$ (M = 430.5 g/mol): Cu, 32.77; C, 19.64; H, 2.75; N, 5.73; S, 6.55. Found: Cu, 32.70; C, 19.62; H, 2.73; N, 5.39; S, 5.27. IR (KBr pellet, cm^{-1}): 746m, 922w, 1029s, 1109m, 1151m, 1187s, 1334m, 1402m, 1507m 1625m, 3436b.

$CoPcTS_0{\subset}Cu$ (2). **$CoPcTS_0Na_4$** (450 mg, 0.46 mmol) was dissolved in 60 mL of water, and the pH was adjusted to 8 using HCl 0.2 M. At this stage, $Cu_2(OH)_3(DS)$ (260 mg, 0.59 mmol) was added along with 20 mL of ethanol, and the mixture was stirred for 8 h at 80 °C under argon. The blue powder was filtered and washed with water and ethanol and dried under vacuum.

Anal. Calcd for $Cu_2(OH)_{3.23}(CoPcTS_0)_{0.19}{\cdot}2.5H_2O$, $Cu_2Co_{0.19}C_{6.08}H_{5.51}N_{1.52}S_{0.76}O_{5.51}{\cdot}2.5H_2O$ (M = 395.9 g/mol): Cu, 32.10; Co, 2.83; C, 18.45; H, 2.68; N, 5.38; S, 6.16. Found: Cu, 32.38; Co, 2.56; C, 18.82; H, 2.59; N, 4.89; S, 5.18. IR (KBr pellet, cm^{-1}): 752m, 932m, 1030s, 1059m, 1109m, 1151m, 1189m, 1329m, 1404m, 1522m, 1629m, 3425b.

$NiPcTS_0{\subset}Cu$ (3). **$NiPcTS_0Na_4$** (450 mg, 0.46 mmol) was dissolved in 100 mL of water, and the pH was adjusted to 8 using HCl 0.2 M. At this stage, $Cu_2(OH)_3(DS)$ (260 mg, 0.59 mmol) was added along with 50 mL of ethanol, and the mixture was stirred for 15 h at 80 °C under argon. The blue-green powder was filtered and washed with water and ethanol and dried under vacuum.

Anal. Calcd for $Cu_2(OH)_{3.2}(NiPcTS_0)_{0.2}{\cdot}2.3H_2O$, $Cu_2Ni_{0.2}C_{6.4}H_{5.6}N_{1.6}S_{0.8}O_{5.6}{\cdot}2.3H_2O$ (M = 400.4 g/mol): Cu, 31.74; Ni, 2.93; C, 19.20; H, 2.57; N, 5.60; S, 6.41. Found: Cu, 31.70; Ni, 2.80; C, 19.18; H, 3.06; N, 5.05; S, 5.28. IR (KBr pellet, cm^{-1}): 750w, 1030s, 1062m, 1107w, 1189m, 1331w, 1404w, 1474w, 1622m, 3443b.

$ZnPcTS_0{\subset}Cu$ (4). **$ZnPcTS_0Na_4$** (454 mg, 0.46 mmol) was dissolved in 100 mL of water, and the pH was adjusted to 8 using HCl 0.2 M. At this stage, $Cu_2(OH)_3(DS)$ (260 mg, 0.59 mmol) was added along with 50 mL of ethanol, and the mixture was stirred for 24 h at 80 °C under argon. The green powder was filtered and washed with water and ethanol and dried under vacuum.

Anal. Calcd for $Cu_2(OH)_{3.16}(ZnPcTS_0)_{0.21}{\cdot}2.5H_2O$, $Cu_2Zn_{0.21}C_{6.72}H_{5.68}N_{1.68}S_{0.84}O_{5.68}{\cdot}2.5H_2O$ (M = 413.6 g/mol): Cu, 30.73; Zn, 3.32; C, 19.51; H, 2.60; N, 5.69; S, 6.51. Found: Cu, 30.93; Zn, 2.59; C, 19.20; H, 3.06; N, 5.60; S, 5.28. IR (KBr pellet, cm^{-1}): 1030s, 1187m, 1335w, 1397w, 1485w, 1627m, 3432b.

$CuPcTS_0{\subset}Co$ (5). **$CuPcTS_0Na_4$** (246 mg, 0.25 mmol) was dissolved in 30 mL of water, and the pH was adjusted to 8 using HCl 0.2 M. At this stage, $Co_2(OH)_3(OAc){\cdot}H_2O$ (248 mg, 1 mmol) was added, and the mixture was stirred for 20 h at 60 °C under argon. The blue powder was collected after four centrifugations (8000 rpm, 10 min each), and the supernatant was replaced after each centrifugation by distilled water in order to wash the product. The collected solid was finally washed with ethanol and dried under vacuum.

dx.doi.org/10.1021/ic4027688 | Inorg. Chem. 2014, 53, 1184−1194

Anal. Calcd for $Co_2(OH)_{3.24}(CuPcTS_0)_{0.19}\cdot 3.8H_2O$, $Co_2Cu_{0.19}C_{6.08}H_{5.52}N_{1.52}S_{0.76}O_{5.52}\cdot 3.8H_2O$ (M = 418.7 g/mol): Co, 28.20; Cu, 2.97; C, 18.0; H, 3.20; N, 5.24; S, 6.00. Found: Co, 28.18; Cu, 2.91; C, 18.06; H, 2.76; N, 4.9; S, 4.26. IR (KBr pellet, cm^{-1}) 743m, 920w, 1028s,1107m, 1150m, 1187m, 1334w, 1397m, 1502m, 1614m, 3447b.

$CoPcTS_0$⊂Co (6). **$CoPcTS_0Na_4$** (245 mg, 0.25 mmol) was dissolved in 60 mL of water, and the pH was adjusted to 8 using HCl 0.2 M. At this stage, $Co_2(OH)_3(OAc)\cdot H_2O$ (248 mg, 1 mmol) was added, and the mixture was stirred for 20 h at 60 °C under argon. The blue powder was filtered and washed with water and ethanol and dried under vacuum.

Anal. Calcd for $Co_2(OH)_{3.2}(CoPcTS_0)_{0.2}\cdot 4.3H_2O$, $Co_{2.2}C_{6.4}H_{5.6}N_{1.6}S_{0.8}O_{5.6}\cdot 4.3H_2O$ (M = 427.3 g/mol): Co, 30.34; C, 17.99; H, 3.35; N, 5.24; S, 6.00. Found: Co, 30.99; C, 17.85; H, 2.94; N, 4.71; S, 4.50. IR (KBr pellet, cm^{-1}): 750m, 933w, 1029s, 1059m, 1109m, 1152m, 1186m, 1330w, 1400w, 1522w, 1622m, 3434b.

$NiPcTS_0$⊂Co (7). **$NiPcTS_0Na_4$** (245 mg, 0.25 mmol) was dissolved in 35 mL of water, and the pH was adjusted to 8 using HCl 0.2 M. At this stage, $Co_2(OH)_3(OAc)\cdot H_2O$ (248 mg, 1 mmol) was added, and the mixture was stirred for 20 h at 60 °C under argon. The blue powder was filtered and washed with water and ethanol and dried under vacuum.

Anal. Calcd for $Co_2(OH)_{3.2}(NiPcTS_0)_{0.2}\cdot 3.5H_2O$, $Co_2Ni_{0.2}C_{6.4}H_{5.6}N_{1.6}S_{0.8}O_{5.6}\cdot 3.5H_2O$ (M = 412.8 g/mol): Co, 28.55; Ni, 2.84; C, 18.62; H, 3.08; N, 5.43; S, 6.21. Found: Co, 28.16; Ni, 2.71; C, 18.81; H, 2.77; N, 5.86; S, 4.05. IR (KBr pellet, cm^{-1}): 1029s, 1061m, 1109w, 1184m, 1331w, 1400w, 1474w, 1609m, 1741w, 3434b.

$ZnPcTS_0$⊂Co (8). **$ZnPcTS_0Na_4$** (247 mg, 0.25 mmol) was dissolved in 60 mL of water, and the pH was adjusted to 8 using HCl 0.2 M. At this stage, $Co_2(OH)_3(OAc)\cdot H_2O$ (248 mg, 1 mmol) was added, and the mixture was stirred for 15 h at 60 °C under argon. The blue powder was filtered and washed with water and ethanol and dried under vacuum.

Anal. Calcd for $Co_2(OH)_{3.44}(ZnPcTS_0)_{0.14}\cdot 5.0H_2O$, $Co_2Zn_{0.14}C_{4.48}H_{5.12}N_{1.28}S_{0.56}O_{5.12}\cdot 5H_2O$ (M = 391.6 g/mol): Co, 30.10; Zn, 2.34; C, 13.74; H, 3.89; N, 4.01; S, 4.59. Found: Co, 29.78; Zn, 1.83; C, 13.65; H, 2.74; N, 3.88; S, 4.98. IR (KBr pellet, cm^{-1}): 1029s, 1186m, 1334w, 1384w, 1484w, 1608m, 3437b.

$CuPcTS_0$⊂Zn (9). **$CuPcTS_0Na_4$** (246 mg, 0.25 mmol) was dissolved in 40 mL of water, and the pH was adjusted to 8 using HCl 0.2 M. At this stage, $Zn_5(OH)_8(DS)_2$ (420 mg, 0.42 mmol) was added along with 25 mL of ethanol, and the mixture was stirred for 24 h at 65 °C under argon. The blue powder was collected after four centrifugations (5000 rpm, 20 min each), and the supernatant was replaced after each centrifugation by a 50/50 v/v water/ethanol mixture in order to wash the product. The collected solid was finally dried under vacuum.

Anal. Calcd for $Zn_5(OH)_8(CuPcTS_0)_{0.5}\cdot 6.5H_2O$, $Zn_5Cu_{0.5}C_{16}H_{14}N_4S_2O_{14}\cdot 6.5H_2O$ (M = 1026.3 g/mol): Zn, 31.86; Cu, 3.10; C, 18.73; H, 2.65; N, 5.46; S, 6.25. Found: Zn, 31.50; Cu, 2.86; C, 19.32; H, 2.47; N, 5.54; S, 5.99. IR (KBr pellet, cm^{-1}): 1029s, 1150m, 1190m, 1337w, 1398w, 1506m, 1629m, 3459b.

RESULTS AND DISCUSSION

Synthesis. The synthesis procedures described here result from significant optimization of the process that we used for insertion-grafting of some metal complexes into layered simple hydroxides. The synthesis of the hybrid compounds was performed using anionic exchange, which is a well-documented method to obtain such hybrid compounds.[16,63−65,67,71−74] Yet, despite repeated efforts, direct intercalation of metal phthalocyanine tetrasulfonate **$MPcTS_0^{4-}$** into copper hydroxyacetate $Cu_2(OH)_3(OAc)\cdot H_2O$ led to a mixture of the starting compounds or to badly crystallized functionalized hybrid lamellar compounds with noticeable quantities of copper oxide CuO. We thus used the preintercalation strategy we have recently described for layered simple hydroxides.[73] This strategy consists in performing the anionic exchange reaction using layered copper hydroxide preintercalated by dodecyl sulfate (DS^-), $Cu_2(OH)_3(DS)$, instead of copper hydroxyacetate.[73,23,24,30] The difficulty to directly insert $MPcTS_0^{4-}$ into the parent copper hydroxy acetate is in line with what has been reported by Hayashi and Hudson, who actually managed to "readily" intercalate the **$CuPcTS_0^{4-}$** anion into $Cu_2(OH)_3(OAc)\cdot H_2O$.[58] Yet, the powder X-ray diffraction pattern of the hybrid compound showed the presence of copper oxide impurities. The mechanism proposed by Hayashi and Hudson consists in the initial intercalation of the phthalocyanines parallel to the layers, followed by their rearrangement to be more perpendicular to the layers.[58,75] However, the real size of the species to be intercalated is strongly dependent on the degree of aggregation of the metal phthalocyanines and thus of the concentration of the starting solution.[32] Therefore, the intercalation of $MPcTS_0^{4-}$ into layered copper hydroxides with small interlamellar spacing is either impossible (for instance, starting from $Cu_2(OH)_3(NO_3)$, which has an interlamellar distance of 0.69 nm[76,77]) or extremely dependent on the reaction conditions (for instance, starting from $Cu_2(OH)_3(OAc)\cdot H_2O$, which has an interlamellar distance of 0.938 nm[78]), giving results rather difficult to reproduce satisfactorily.

The preintercalation strategy enables us to overcome these difficulties by increasing considerably the interlamellar space available (2.67 nm for $Cu_2(OH)_3(DS)$)[67] and by providing hydrophobic interlamellar environment, which may reduce the sensibility toward oxidation during the insertion reaction.[79] Four hybrid layered copper hydroxides functionalized by **$MPcTS_0^{4-}$** were obtained and characterized: **$CuPcTS_0$⊂Cu** (**1**), **$CoPcTS_0$⊂Cu** (**2**), **$NiPcTS_0$⊂Cu** (**3**), and **$ZnPcTS_0$⊂Cu** (**4**). It is worth emphasizing here the importance of the temperature of the insertion reaction. The use of temperatures lower than 70 °C leads to monophasic compounds, but in which the exchange of the dodecylsulfate anion remains partial, for any duration of reaction.[80] Finally, copper phthalocyanine tetrasulfonate **$CuPcTS_0^{4-}$** was inserted into layered zinc hydroxide using the same preintercalation strategy (**$CuPcTS_0$⊂Zn** (**9**)).

For the cobalt hydroxide-based compounds, direct insertion of **$MPcTS_0^{4-}$** into $Co_2(OH)_3(OAc)\cdot H_2O$ led to the desired hybrids with good yields (**$CuPcTS_0$⊂Co** (**5**), **$CoPcTS_0$⊂Co** (**6**), **$NiPcTS_0$⊂Co** (**7**), and **$ZnPcTS_0$⊂Co** (**8**)). The use of the preintercalated compound $Co_2(OH)_3(DS_0)\cdot H_2O$ (DS_0^- = dodecylsulfonate) as a starting material generates the same compounds. This difference, both in reactivity (necessary ratio between reactants) and in mechanism (preintercalation or not), suggests different insertion-grafting mechanisms in the two lamellar hosts, exhibiting different structures of the inorganic sheets. The process is mainly topotactic in the case of copper hydroxide, although some small variation of the inorganic layer structure may occur because of the necessary adaptation of the metal layer to the molecular area of the grafted anions;[81] however, dissolution−recrystallization occurs in the case of cobalt hydroxide.[65,82]

Finally, there was no difference neither in the reaction conditions nor in the obtained hybrid compounds whether the phthalocyanine used were sulfonated in 3,4′,4″,4‴ or in 4,4′,4″,4‴ positions.

The different reaction conditions are summarized in Table S1. Elemental analyses carried out on all compounds **1**−**8** are in accordance with the general formula $M_2(OH)_{4-4x}(M'PcTS_0)_x\cdot$

dx.doi.org/10.1021/ic4027688 | Inorg. Chem. 2014, 53, 1184−1194

zH_2O, with x around 0.2 and z ranging from 2.3 to 5. For **9**, the elemental analysis brings about the formula $Zn_5(OH)_8(CuPcTS_0)_{0.5}\cdot 6.5H_2O$, in accordance with the structure of layered Zn hydroxide hybrids (see below). It is worth noting that the elemental analyses show no evidence of any remaining dodecyl sulfate or acetate molecules, using the present insertion conditions.

X-ray Diffraction. PXRD patterns of the hybrid compounds **1**−**9** show intense *00l* diffraction lines in the low 2θ region, up to at least the third harmonic, which is characteristic of their lamellar structure (Figures 1, S1 and S2). After the anion-exchange reaction, all products show an abrupt change of the *00l* peak position, which indicates that the insertion of a new species actually occurred. No diffraction lines coming from the starting materials were present, indicating the completeness of the reactions. All compounds based on a given metal hydroxide have the same basal spacing around 2.1 nm for copper hydroxide-based compounds, around 2.2 nm for cobalt hydroxide-based compounds, and around 2.1 nm for the zinc hydroxide-based compound (Table 1).

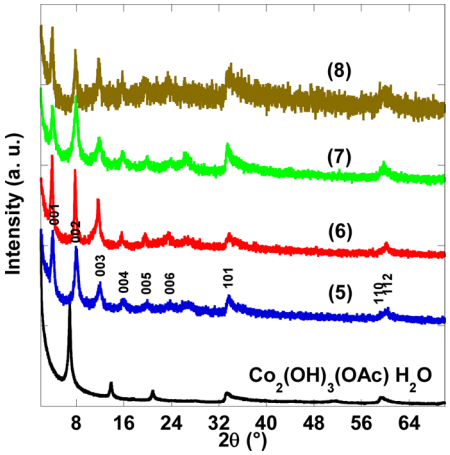

Figure 1. PXRD patterns of the cobalt hydroxide-based compounds: **CuPcTS$_0$⊂Co** (**5**), **CoPcTS$_0$⊂Co** (**6**), **NiPcTS$_0$⊂Co** (**7**), and **ZnPcTS$_0$⊂Co** (**8**) along with the starting $Co_2(OH)_3(OAc)\cdot H_2O$ (Cu Kα_1 = 0.1540598 nm). Indexation of the diffraction peaks corresponds to a hexagonal unit cell $a \approx 3.12$ Å and c as reported in Table 1 (see text).

With respect to the thickness of the copper, cobalt, and zinc hydroxide layers (0.29, 0.73, and 0.72 nm, respectively),[67,83] the basal spacing is in good agreement with the size of the phthalocyanine complexes (about 1.99 × 1.73 × 0.55 nm^3).[48] The basal spacings observed are consistent with phthalocyanine complexes grafted almost perpendicularly to the copper hydroxide layers (tilted by less than 15°) and with a tilt angle of about 35° in the case of cobalt and zinc hydroxides. A model structure of the cobalt hydroxide-based hybrids is schematized in Figure 2. The structure of the cobalt hydroxide layers is typical of hydrozincite. Nevertheless, if hydrozincite is a good model to represent the structure of the present compounds, the actual structure is merely a disordered variation, with a statistical distribution of the tetrahedral sites. Such a disordered structure was suggested for α-cobalt hydroxide, cobalt hydroxychloride, and cobalt hydroxycarbonates on the basis of synchrotron X-ray data and neutron analysis. The structures of these compounds were refined in a hexagonal $R\bar{3}m$ system.[84−86]

Table 1. Interlamellar Spacing of the Hybrid Compounds 1−9

	interlamellar spacing (nm)
CuPcTS$_0$⊂Cu (**1**)	2.11(1)
CoPcTS$_0$⊂Cu (**2**)	2.07(2)
NiPcTS$_0$⊂Cu (**3**)	2.13(2)
ZnPcTS$_0$⊂Cu (**4**)	2.13(2)
CuPcTS$_0$⊂Co (**5**)	2.22(3)
CoPcTS$_0$⊂Co (**6**)	2.26(2)
NiPcTS$_0$⊂Co (**7**)	2.23(2)
ZnPcTS$_0$⊂Co (**8**)	2.25(5)
CuPcTS$_0$⊂Zn (**9**)	2.17(2)

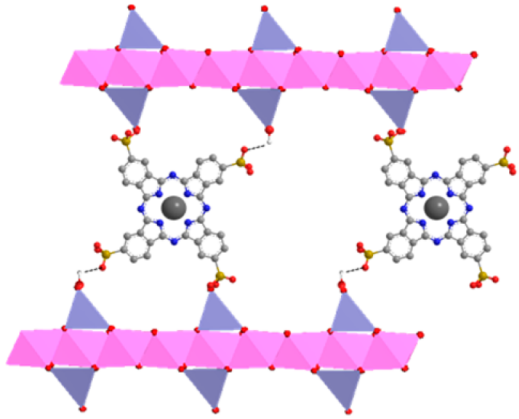

Figure 2. Schematic representation of the structure of compounds **5**−**8**.

Finally, the XRD patterns of all cobalt hydroxide compounds including the starting acetate $Co_2(OH)_3(OAc)\cdot H_2O$ exhibit similar features in the region of in-plane diffraction lines (high 2θ angles) with characteristic asymmetrical peaks at 2θ = 33° and 2θ = 59° (Cu Kα_1 = 0.1540598 nm). Such asymmetry suggests turbostratic disorder. We collected essentially *00l* diffraction lines and very few lines giving information on the in-plane parameters. We tentatively indexed the patterns in Figure 1 on the basis of a hexagonal unit cell with a around 3.12 Å evaluated from the peaks around 2θ = 60° and c as evaluated from the *00l* lines. This is consistent with the hexagonal unit cells found for α-cobalt hydroxide, cobalt hydroxychloride, and cobalt hydroxycarbonates.

Infrared Spectroscopy. FTIR spectra of the compounds **1**−**9** (Figures S3, S4, and S5) show that the bands characteristic of the molecules initially present in the interlamellar space of the starting compounds totally vanished after the exchange reaction (i.e., the bands of acetate in the case of cobalt hydroxide and of dodecyl sulfate in the case of copper and zinc hydroxides). The absence of acetate anions is clearly evidenced by the absence of the COO^- elongation vibrations around 1550 and 1400 cm^{-1}. The absence of the dodecyl sulfate chains is evidenced by the very low intensity of the CH_2 elongation vibrations (2924 and 2853 cm^{-1}). Moreover, the complete removal of the dodecyl sulfate or acetate moieties for compounds **1**−**9** upon exchange by the phthalocyanine sulfonate complexes was confirmed by elemental analysis (see the Experimental Section). Finally, the low energy region clearly shows the bands corresponding to the phthalocyanine complexes, indicating a successful insertion (Table 2). The

dx.doi.org/10.1021/ic4027688 | Inorg. Chem. 2014, 53, 1184−1194

Table 2. Position of Some Vibrational Absorption Bands for the Starting Complexes and for the Hybrid Compounds 1−9 (cm^{-1})

	νC−N (cm^{-1})	$\nu_{isoindole}$ (cm^{-1})	ν_sC−C (cm^{-1})	$\nu_{as}SO_3^-$ (cm^{-1})	ν_s SO_3^- (cm^{-1})	$\Delta\nu$ (cm^{-1})
MPcTs$_0$Na$_4$ (M = Cu, Co, Ni, Zn)	1480−1505	1390−1400	1330	1189	1030	159
CuPcTS$_0$⊂Cu (**1**)	1507	1398	1337	1188	1029	159
CoPcTS$_0$⊂Cu (**2**)	1524	1404	1331	1189	1030	159
NiPcTS$_0$⊂Cu (**3**)	1522[a]	1407	1333	1189	1030	159
ZnPcTS$_0$⊂Cu (**4**)	1485	1397	1335	1187	1030	157
CuPcTS$_0$⊂Co (**5**)	1507	1396	1340	1187	1029	158
CoPcTS$_0$⊂Co (**6**)	1522	1402	1331	1186	1029	157
NiPcTS$_0$⊂Co (**7**)	1541[a]	1403	1333	1185	1029	156
ZnPcTS$_0$⊂Co (**8**)	1484	1384	1334	1186	1029	157
CuPcTS$_0$⊂Zn (**9**)	1506	1398	1337	1190	1029	161

[a]Poorly resolved.

C═C elongation vibration around 1630 cm^{-1} cannot be identified precisely, due to strong overlap with the water bending vibration. Between 1530 and 1300 cm^{-1}, three absorption bands can be identified, corresponding to C−N pyrrole, isoindole, and C−C pyrrole elongation vibrations.[31,56]

The identification of the asymmetric and symmetric vibrations of the sulfonate groups is important to precisely determine the coordination of the ligands.[73,87−90] In the present case, two stretching vibrations of SO_3^- are observed as a sharp peak around 1030 cm^{-1} and a broader one around 1190 cm^{-1}, which is attributed to the symmetric and asymmetric vibration modes, respectively. For the hybrid compounds, $\Delta\nu$ ($\Delta\nu = \nu_{asym} - \nu_{sym}$) is almost identical to the one observed for the free sulfonato phthalocyanine anions. A $\Delta\nu$ value lower that the one of the free ligand indicates noncoordination to the inorganic layer, whereas a higher one indicates monocoordination of the sulfonate group to the inorganic layers.[57,88−90] Here, the situation is intermediate, which, considering the broadness of the asymmetric streching band of the sulfonates, may indicate that some of the four sulfonate groups borne by the phthalocyanines are coordinated, whereas some are not directly linked to the metal ion of the inorganic layers but involved in hydrogen bonds, as in LDH compounds or some NiLSH.[88]

UV−Vis Spectroscopy. The main and most characteristic feature of the absorption spectra of the phthalocyanines is the presence of two very intensive bands, called Q- and B-bands (at about 670 and 350 nm, respectively) and both attributed to $\pi-\pi^*$ macrocyclic ring transition.[32]

The spectra of the hybrid compounds present similar features, supporting the presence of the phthalocyanine complexes (Figures 3, S6 and S7). The Q-band is slightly shifted toward higher energy in the hybrids with respect to its position in the **MPsTS$_0^{4-}$** ion alone. For instance, the Q-band of **CuPcTS$_0^{4-}$** is around 580 nm in the hybrids, whereas it is at 600 and 630 nm for **CuPcTS$_0$Na$_4$** in the solid state and in solution in water (2×10^{-6} mol·L^{-1}), respectively. This blue shift of the Q-band suggests near or full cofacial alignment of two or more phthalocyanine molecules in the interlamellar space of the layered hybrids.[91−93]

Lastly, the electronic transitions of the phthalocyanine complexes partially overlay the transitions arising from the inorganic structures. In the UV region, the O→M charge transfer (M = Co or Cu) of the inorganic layers is superimposed upon the B-band of the phthalocyanine. For the cobalt hybrids (**5**-**8**), two additional bands are observed in the NIR region around 1190 and 1450 nm. These bands are attributed to electronic d−d transitions of d^7 Co(II) ions, in

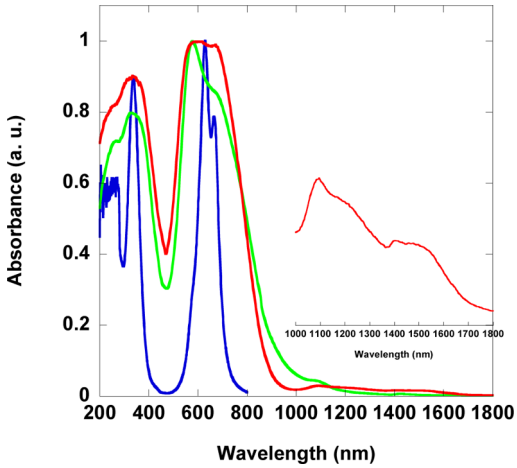

Figure 3. UV−vis NIR absorption spectra of **CuPcTS$_0$⊂Cu** (**1**) (green), **CuPcTS$_0$⊂Co** (**5**) (red) (solid state), and **CuPcTS$_0$Na$_4$** (blue) (2×10^{-6} mol·L^{-1} in water).

octahedral ($^4T_{1g}(F) \rightarrow {}^4T_{2g}(F)$) and tetrahedral sites ($^4A_2(F) \rightarrow {}^4T_1(F)$), respectively.[94] These features are consistent with the proposed structure of the inorganic layers and with the magnetic behavior (see below).[72,95] Two additional transitions are expected at higher energies (around 580 and 630 nm), corresponding, respectively, to the $^4T_{1g}(F) \rightarrow {}^4T_{1g}(P)$ transition of Co(II) in octahedral site and to the $^4A_2(F) \rightarrow {}^4T_1(P)$ transition of Co(II) in tetrahedral site. These two transitions are not observed here because they are masked by the Q-band of the phthalocyanine complexes.

For the **MPcTs$_0$⊂Cu** hybrid (**1**-**4**), the expected $^2E_g \rightarrow {}^2T_{2g}$ transition of Cu(II) ions in octahedral geometry is masked by the Q-band as well.

Magnetic Properties. The magnetic properties of the copper hydroxide-based compounds are rather similar (Figure 4, S11 and S12). The Curie constants deduced using the Curie−Weiss law (1.06, 1.03, 0.86, and 0.75 emu·K·mol^{-1} for **1**, **2**, **3**, and **4**, respectively) are in agreement with the expected values (around 0.9 emu·K·mol^{-1} for **1** and **2** and around 0.8 emu·K·mol^{-1} for **3** and **4**) considering C ∼ 0.8 emu·K·mol^{-1} for the two Cu(II) ions of the inorganic layer,[73] and C = 0.39 emu·K·mol^{-1} and 0.44 emu·K·mol^{-1} for **CuPcTS$_0^{4-}$** and **CoPcTS$_0^{4-}$**, respectively.[69] (**NiPcTS$_0^{4-}$** and **ZnPcTS$_0^{4-}$** are diamagnetic.) The uniform decrease of χT versus T curves with temperature indicates the predominance of antiferromagnetic interactions.

dx.doi.org/10.1021/ic4027688 | Inorg. Chem. 2014, 53, 1184−1194

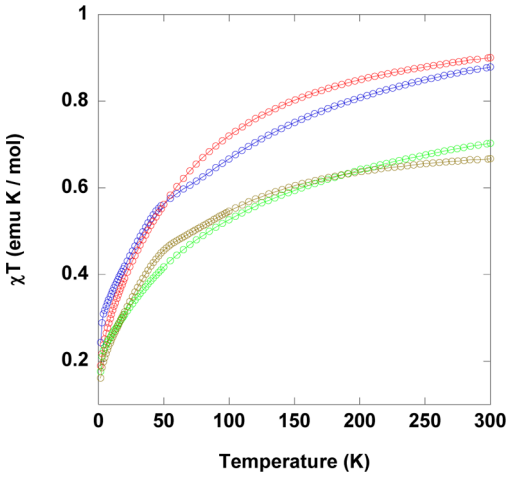

Figure 4. $\chi T = f(T)$ under a 5000 G applied dc field for **CuPcTS$_0$⊂Cu** (**1**) (blue), **CoPcTS$_0$⊂Cu** (**2**) (red), **NiPcTS$_0$⊂Cu** (**3**) (green), and **ZnPcTS$_0$⊂Cu** (**4**) (brown) (full lines are only guides for the eye).

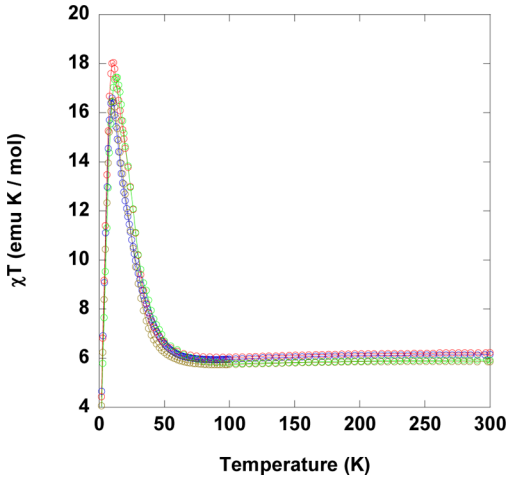

Figure 5. $\chi T = f(T)$ under a 5000 G applied dc field for **CuPcTS$_0$⊂Co** (**5**) (blue), **CoPcTS$_0$⊂Co** (**6**) (red), **NiPcTS$_0$⊂Co** (**7**) (green), and **ZnPcTS$_0$⊂Co** (**8**) (brown) (full lines are only guides for the eye).

Magnetization versus field measurements at 1.8 K (Figure S11) shows a rather slow increase at low field, with a high-field magnetization far from saturation and much lower than the expected value for full alignment of the moments of the paramagnetic ions. The ac susceptibility measurements (Figure S12) are identical for all compounds, and only bases of growing peaks in the χ' and χ'' signals were observed for **1**−**4**, indicating that there is no long-range order down to 1.8 K. This behavior is similar to the one observed for the starting $Cu_2(OH)_3(DS)$.[65] Two hypotheses can explain the behavior. The coupling between the spin carriers within the inorganic planes may be antiferromagnetic, resulting in an overall antiferromagnetic behavior. Or, the coupling within the plane leads to a resulting moment (weak canting or ferrimagnetism), and for anisotropy reasons, this moment is aligned within the inorganic plane. This situation leads to an antiferromagnetic coupling between the planes due to dipolar interaction.[96] Yet, in the absence of additional structural information, it is not possible to go further in the interpretation of the magnetic behavior.

The magnetic behaviors of the cobalt hydroxide-based compounds are also very similar. The Curie constants (6.23, 6.32, 6.03, and 5.93 emu·K·mol^{-1} for **5**, **6**, **7**, and **8**, respectively) are consistent with the presence of the phthalocyanine complexes and a mixture of tetrahedral and octahedral high-spin Co(II) ions with $C_{tetra} \sim 2.2$ - 2.8 emu·K·mol^{-1} and $C_{octa} \sim 3.2$ emu·K·mol^{-1}.[72,73,97,98] Upon cooling, the χT product for the four cobalt hybrids shown in Figure 5 decreases regularly down to a minimum at around 100 K (from 6.13 emu·K·mol^{-1} at 300 K to 5.94 emu·K·mol^{-1} at 89 K for **5**, 6.22 emu·K·mol^{-1} at 300 K to 6.04 emu·K·mol^{-1} at 95 K for **6**, 5.93 emu·K·mol^{-1} at 300 K to 5.79 emu·K·mol^{-1} at 109 K for **7**, and 5.86 emu·K·mol^{-1} at 300 K to 5.74 emu·K·mol^{-1} at 92 K for **8**). This small decrease is well understood as a result of spin−orbit coupling effect and/or antiferromagnetic interactions between the Co(II) moments. Below this minimum, the χT products for **5**−**8** exhibit a steep increase to a maximum at 10.1 K (16.6 emu·K·mol^{-1}) for **5**, 10.9 K (18.1 emu·K·mol^{-1}) for **6**, 13.0 K (17.4 emu·K·mol^{-1}) for **7**, and 10.0 K (16.6 emu·K·mol^{-1}) for **8** (all measurements were performed under an applied dc field of 0.5 T). This steep increase can be related to the occurrence of long-range ferromagnetic correlations.

Ordering temperatures were determined by ac susceptibility measurements (Figure 6). The maximum of the real part χ'

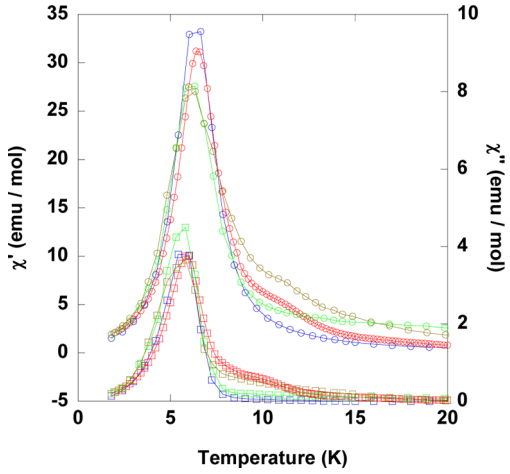

Figure 6. In-phase (open circles) and out-of-phase (open squares) susceptibility measurements (0 T dc field, 0.35 mT oscillating field, f = 95 Hz) for **CuPcTS$_0$⊂Co** (**5**) (blue), **CoPcTS$_0$⊂Co** (**6**) (red), **NiPcTS$_0$⊂Co** (**7**) (green), and **ZnPcTS$_0$⊂Co** (**8**) (brown) (full lines are only guides for the eye).

leads to T_N = 6.6 K for **5**, 6.4 K for **6**, 6.3 K for **7**, and 6.3 K for **8**. The ferromagnetic behavior of compounds **5**−**8** was confirmed by the magnetization versus field curves at low temperature (Figure 7), which exhibit hysteresis loops with almost identical coercive fields of 65 mT at 1.8 K for **5**, **7**, and **8** and 47 mT for **6** and remnant magnetization around 1.1 μ_B at 1.8 K for all compounds. The low value of the moments at high field (around 3.4 μ_B at 5 T and 1.8 K) compared to the expected value for a total alignment of the moments (4−6 μ_B for two Co(II) and about 1 μ_B per Cu or Co phthalocyanine), supports a ferrimagnetic ordering. As observed in other layered cobalt simple hydroxides,[17,97] we can assume that this ferrimagnetic ordering results from unbalanced antiparallel alignment of the moments borne by tetrahedral and octahedral Co(II) ions. This behavior is similar to the one of the starting compound $Co_2(OH)_3(OAc)·H_2O$, which presents a ferrimagnetic ordering at T_N = 18 K.[99] The difference of the ordering

dx.doi.org/10.1021/ic4027688 | Inorg. Chem. 2014, 53, 1184−1194

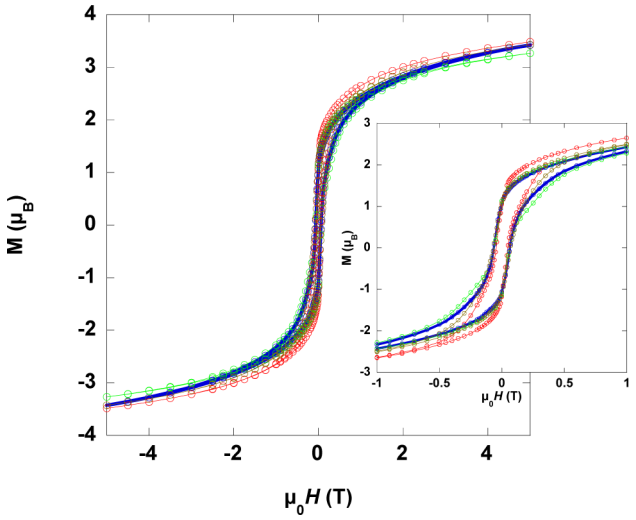

Figure 7. $M = f(H)$ at 1.8 K for **CuPcTS$_0$⊂Co** (**5**) (blue), **CoPcTS$_0$⊂Co** (**6**) (red), **NiPcTS$_0$⊂Co** (**7**) (green), and **ZnPcTS$_0$⊂Co** (**8**) (brown) (full lines are only guides for the eye).

temperature is due to the modification of the inorganic layer induced by the grafting of the phthalocyanine complexes, resulting in a change on the 2D magnetic correlation domains.[65]

The important point which is worth noting here is that there is almost no difference in the magnetic properties of the various cobalt hydroxide-based hybrids regardless of the transition metal present in the phthalocyanine complex inserted. This indicates that the complexes bridging the layers do not participate in the establishment of the magnetic ordering. This feature was already observed in the case of salen-type complexes anchored via sulfonate groups in LSH.[23,30] Therefore, the magnetic interaction between the inorganic layers can be considered here as purely dipolar.[96,99−101]

Electron Paramagnetic Resonance Spectroscopy. To support the interlayer mechanism of coupling that we suggest, the behavior of the paramagnetic phthalocyanines inserted was characterized by means of EPR spectroscopy performed at X-band ($\nu \sim 9.8$ GHz) and Q-band ($\nu \sim 34$ GHz). The lack of resolution of anisotropic g-tensors may be overcome at least partially upon applying a higher frequency, which splits up the different resonance fields.

We focus here on the compounds functionalized with the Cu(II) phthalocyanine complex (**1**, **5**, **9**), which will be compared when necessary with the compounds involving the Ni(II) and Zn(II) phthalocyanine complexes (**3**, **4**, **7**, **8**). Due to the specificity of the EPR behavior of Co(II), detailed analysis of the behavior of the compounds functionalized by the Co(II) phthalocyanine (**2** and **6**) will be published elsewhere.[102] Measurements were carried out on polycrystalline powder samples.

X-Band. The X-band EPR spectra of **CuPcTS$_0$Na$_4$** and of **CuPcTS$_0$⊂Zn** (**9**) exhibit a single line close to Lorentzian shape centered at $g_{iso} = 2.05$ in accordance with commonly reported shapes and values for Cu(II) phthalocyanines (Figure S13).[25,103−107] The position of the peak and the peak-to-peak line width ($\Delta B_{pp} = 10$ mT) are temperature independent. The absence of hyperfine structure in the EPR spectra of the phthalocyanine, either in its native form or intercalated in a layered host (contrarily to what has been observed for Cu(II) phthalocyanines inserted into zeolite-Y with a high Si/Al ratio[47]), is probably due to intermolecular interactions between phthalocyanines.[25,107]

The EPR spectrum of **CuPcTS$_0$⊂Cu** (**1**) is similar to the ones of **9** and of **CuPcTS$_0$Na$_4$** (Figure S13). It exhibits a single line centered at $g_{iso} = 2.05$, the position and peak-to-peak line width of which ($\Delta B_{pp} = 10$ mT) are also temperature independent. The spin concentration calculated from the double integration of the EPR spectrum of **1** is about 10^{23} spins·mol^{-1}. To identify and then to subtract a possible contribution of the Cu-hydroxide layers, the EPR spectrum of **NiPcTS$_0$⊂Cu** (**3**) (identical to the one of **ZnPcTS$_0$⊂Cu** (**4**)) has been recorded (Figure S14). The Cu(II) layers are essentially EPR-silent due to strong antiferromagnetic interactions. The very low spin concentration ($\approx 10^{17}$ spins·mol^{-1}) and the observation of the parallel components of the hyperfine tensor allow concluding that the only weak EPR contribution observed originates from uncoupled Cu(II) species within the Cu-hydroxide layers.

As for the Co(II)-hydroxide derivatives, the X-band experimental spectra of **CuPcTS$_0$⊂Co** (**5**) and of **NiPcTS$_0$⊂Co** (**7**) (identical to the one of **ZnPcTS$_0$⊂Co** (**8**)), recorded at 4.3 K, are presented in Figure 8, together with simulated spectra.

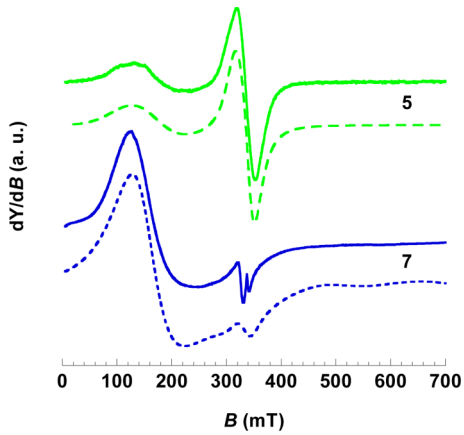

Figure 8. X-band EPR spectra ($T = 4.3$ K) of powder samples of **CuPcTS$_0$⊂Co** (**5**) ($\nu = 9.391$ GHz) and **NiPcTS$_0$⊂Co** (**7**) ($\nu = 9.391$ GHz); experimental (upper trace) and simulation (lower trace, dashed line) (simulation parameters are reported in Supporting Information, Table S2).

Given that **NiPcTS$_0$$^{4-}$** is diamagnetic, the X-band EPR spectrum of **7** solely signs a high spin $S = 3/2$ Co(II) ion. Such an HS Co ion is usually recognized by poorly resolved resonances lines broadened by a combination of large g-anisotropy, sizable spin−orbit coupling and a mixture of excited state character into the magnetic ground state.[108−110] The sharp line at $g = 1.99$ likely arises from impurities of NiPc$^{\bullet}$ radical. The larger weak signal around $g = 2$ is due to the resonator. Both of them account for less than 1% of the overall EPR signal of **7**.

The EPR spectrum of **CuPcTS$_0$⊂Co** (**5**) shows two well-separated peaks, which, according to the experiments performed on the reference compounds described above, are easily ascribed to: (i) the high-spin octahedral Co(II) constituting the layers for the low-field component and (ii) the inserted **CuPcTS$_0$$^{4-}$** for the sharper line centered around 330 mT. The spin concentration of the signal attributed to the Cu phthalocyanine is about 4×10^{22} spins·mol^{-1}, in very good

dx.doi.org/10.1021/ic4027688 | Inorg. Chem. 2014, 53, 1184−1194

agreement with the proposed formula for **5**. The temperature dependence of the X-band EPR spectrum (Figure 9) shows a

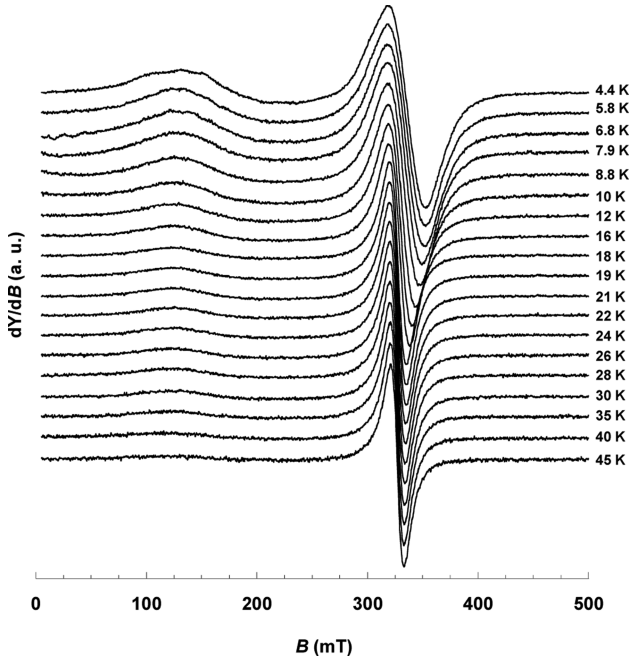

Figure 9. X-band EPR spectra **CuPcTS$_0$⊂Co** (**5**) as a function of temperature (ν = 9.391 GHz).

striking broadening and a shift toward high fields of the Cu phthalocyanine line below ≈20 K. None of these features was observed in the case of **1** and **9**; therefore, this behavior in **5** is necessarily a consequence of the magnetic ordering of the compound. The Cu phthalocyanine complex acts as a paramagnetic probe of the internal field of the compound when it gets magnetically ordered. However, X-band EPR spectra are not resolved enough to allow precise discussion of this behavior. Hence, Q-band EPR spectroscopy experiments have been performed to analyze in more detail the peculiar features of the thermal evolution of the spectra (e.g., line broadening versus *g*-shift).

Q-Band. Q-band EPR spectroscopy enables the resolution of the anisotropy of the Cu phthalocyanine complexes. We focus here on the $g \sim 2$ region of the spectra of **1**, **5**, and **9**. The Q-band EPR spectra of these three compounds are similar at 90 K (Figure 10). They sign a Cu(II)-ion in a planar configuration with an axial *g*-tensor with principal values that are consistent with those reported for isolated **CuPcTS$_0$Na$_4$** in solution[111−113] or with those deduced from the Q-band EPR spectrum of a powdered sample of **CuPcTS$_0$Na$_4$** (Figure S15). The variations of the line width and the resulting line shape are mostly due to the unresolved hyperfine couplings, being more important at $g_{//}$ than at $g_{\perp}$. Simulation of the EPR spectra has been performed with EasySpin software[70] where B_{strain} stands for the residual line width describing broadening due to unresolved hyperfine couplings. The two components are the Gaussian linewidths in the perpendicular and parallel directions of the molecular frame. The spectra of **1**, **5**, and **9** at 90 K can be simulated with close parameters. Simulated spectra yield $g_{//} = 2.150 \pm 0.005$; $g_{\perp} = 2.040 \pm 0.003$; $B_{strain//} = 50 \pm 2$ mT; $B_{strain\perp} = 13 \pm 1$ mT; line width =10 ± 1 mT. (Specific simulation parameters for each spectrum are reported in Supporting Information.) The unresolved large parallel B_{strain} ($B_{strain//}$) required for the

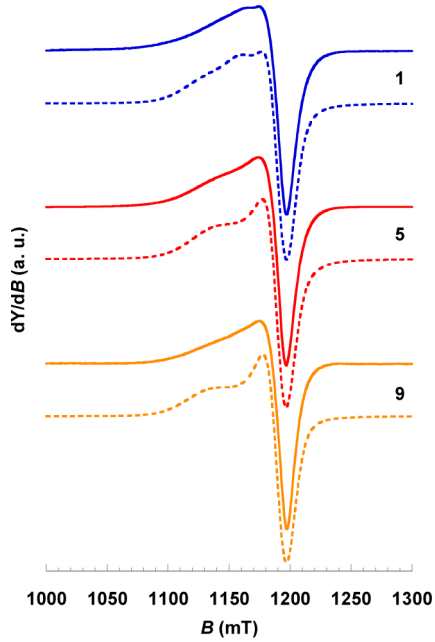

Figure 10. Q-band EPR spectra of powder samples of **CuPcTS$_0$⊂Cu** (**1**) (ν = 34.073 GHz), **CuPcTS$_0$⊂Co** (**5**) (ν = 34.034 GHz), and **CuPcTS$_0$⊂Zn** (**9**) (ν = 34.080) at 90 K; experimental (upper trace) and simulation (lower trace, dashed line) (simulation parameters are reported in Supporting Information, Table S3).

numerical simulation accounts well for a typical parallel contribution of the hyperfine tensor of a ^{63}Cu nucleus (≈3 × 17 mT).[111−113] The flat shape of the parallel region is possibly due to the existence of intermolecular interactions between neighboring phthalocyanines, leading to a broadening of the spectra in the parallel region. It thus comes about that the perpendicular part of the spectra is more suitable and precise for discussion, thus confirming the advantage in terms of resolution of the Q-band over the X-band.

Q-band EPR spectra of **1**, **5**, and **9** have been recorded at various temperatures between 90 and 5 K to be compared to similar studies at X-band (Figures 10, 11 and S16). Whereas for **1** and **9** the parameters obtained from the simulation hardly change, for **5**, considerable line broadening and resonance shift are observed as the temperature decreases.

It appears that between 90 and 5 K, the position of the perpendicular resonance for **CuPcTS$_0$⊂Co** (**5**) is shifted toward high fields by ≈30 mT. This is concomitant with a drastic line broadening from 10 mT at 90 K up to ≈66 mT at 5 K (Figure 12).

Magnetic measurements have shown that **1** exhibits antiferromagnetic interactions without ordering and **5** orders ferrimagnetically with a critical temperature of ≈6 K, identical for any particular nature of phthalocyanine complex inserted. EPR experiments ascertain that the fingerprint of the Cu phthalocyanine remains unchanged while sandwiched between diamagnetic Zn hydroxide-based layers. Moreover, a temperature-independent EPR signal of **CuPcTS$_0$** is observed as well in **1**. This corroborates the absence of magnetic exchange between Cu hydroxide-based layers and the **CuPcTS$_0$** guest. Therefore, assuming also the lack of direct magnetic exchange between **CuPcTS$_0$** and Co hydroxide-based layers in compound **5** (which is confirmed by the invariance of the ordering temperature upon the nature of the inserted metal phthalocyanine complex), the line broadening and resonance

dx.doi.org/10.1021/ic4027688 | Inorg. Chem. 2014, 53, 1184−1194

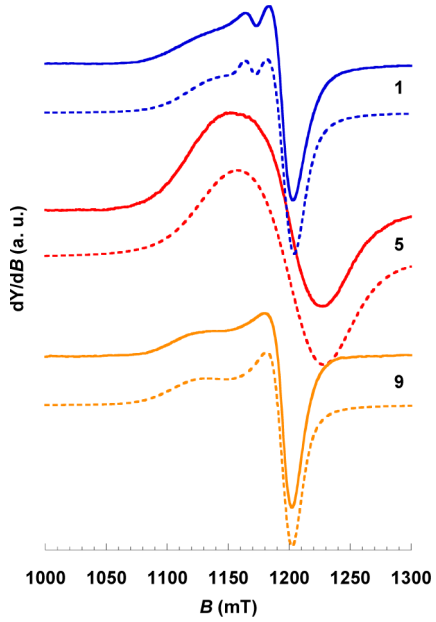

Figure 11. Q-band EPR spectra of powder samples of **CuPcTS$_0$⊂Cu** (**1**) (ν = 33.996 GHz), **CuPcTS$_0$⊂Co** (**5**) (ν = 33.941 GHz), and **CuPcTS$_0$⊂Zn** (**9**) (ν = 34.043 GHz) at 5 K; experimental (upper trace) and simulation (lower trace, dashed line) (simulation parameters are reported in Supporting Information, Table S3).

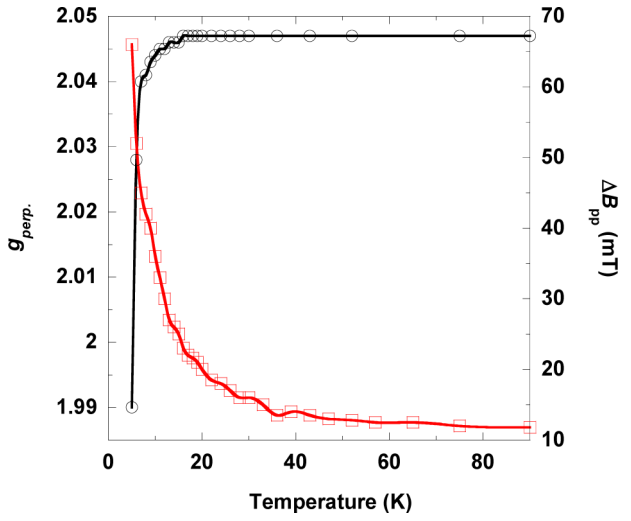

Figure 12. Temperature dependence of the Cu phthalocyanine component of the Q-band EPR spectra of **CuPcTS$_0$⊂Co** (**5**): line width, ΔB_{pp} (open squares), and $g_\perp$ (open circles) (full lines are only guides for the eye).

shift noticed for **5** when decreasing temperature can be ascribed solely to the dipolar field growing between the Co hydroxide layers. As previously suggested,[96,100] the magnetic ordering in **5** takes place due to dipole−dipole interaction between "giant spins", corresponding to 2D correlation domains growing within the Co hydroxide layers. A local field is concomitantly created that superimposes to the applied Zeeman field of EPR. The contribution of this additional field may be roughly estimated from the shift of $g_\perp$ between 90 and 5 K: $B_{dipolar} \approx 30$ mT.

The paramagnetic phthalocyanine acts as a probe, which is sensitive to the internal field that develops when the material gets magnetically ordered. In the present case, this internal field is subtracted from the applied field, so as to increase the resonance field. A similar feature was already observed in the case of the insertion-grafting of nitroxide radical species into Co hydroxide layers.[63] The present result seems opposite to the one recently observed for magnetic layered double hydroxides.[25] In that case, however, it is likely that the overly low resolution of X-band EPR spectroscopy prevented the precise study of the evolution of the parallel and perpendicular components of the transition. Our point is that the value of the internal field determined here is of the same order of magnitude compared to the one determined in the case of the insertion of the radical species into Co hydroxide layers.[63] In the latter compounds, the internal field experienced by the radical species was that of the dipolar field, but the radicals were also involved in an interlamellar exchange pathway with significant Co(II)-radical and radical−radical couplings. In the present compounds, such exchange interaction through the phthalocyanine complexes is ruled out by the magnetic findings. To our knowledge, it is the first time the value of a purely dipolar internal field developing between magnetic layered simple hydroxides is reported.

CONCLUSION

We have described here the synthesis and properties of a series of new Cu, Co, and Zn layered simple hydroxides functionalized by Cu, Ni, Co, and Zn phthalocyanine tetrasulfonate complexes. These compounds are among the rare examples of LSHs functionalized by transition metal complexes. In the case of Cu and Zn layered hydroxides, the insertion-grafting of the phthalocyanine complexes occurs via preinsertion of dodecyl sulfate, whereas in the case of Co layered hydroxide, it takes place from the starting Co hydroxyacetate. All compounds, for a given metal hydroxide, are isostructural, with similar interlamellar distances, regardless of the nature of the metal phthalocyanine inserted. Such a strategy enables us to tune the electronic structure of the inserted species without modifying the structure of the layered host.

Whereas all Cu hydroxide-based compounds present an overall antiferromagnetic behavior, the Co hydroxide-based compounds show a ferrimagnetic ordering at about 6.4 K, without any influence of the nature of the metal phthalocyanine complex on the magnetic properties of the hybrid. The lack of significant coupling between the inorganic host and the molecular guest is explained by the use of sulfonate moieties as coordinating functions. Sulfonates are indeed known to be weak mediators of magnetic interactions.[114] This enables us to assert the strictly dipolar nature of the interaction between the magnetic hydroxide layers. The inserted Cu or Co phthalocyanine complexes act thus as innocent paramagnetic probes of the internal dipolar field, which has been determinated by X- and Q-band EPR spectroscopy studies ($B_{dipolar} \approx 30$ mT).

This investigation states quantitatively the mechanisms responsible for the magnetic ordering in these layered hybrids. This is of utmost importance for the further design of magnetic LSH-based multifunctional systems and more generally of magnetic hybrid multilayers, especially when interaction between the properties of the subnetworks is sought after. For instance, as stated in the introduction, the design of magneto-luminescent or magneto-chiral compounds by functionalization of layered hydroxide-based magnets using different coordination functions is currently an active field of research.

dx.doi.org/10.1021/ic4027688 | Inorg. Chem. 2014, 53, 1184−1194

Finally, we would like to emphasize that beyond their magnetic properties, the materials reported in this paper constitute a new family of hybrid magnetic materials in which transition metal complexes are immobilized. This constitutes a tractable and appealing way toward new multifunctional materials with properties brought by the inserted phthalocyanine complexes, like photoluminescence or catalysis of the oxygen reduction reaction. With regard to the properties of the compounds described here, the electrochemical activity of the LSHs functionalized by Co phthalocyanine is under study. Preliminary results show that these hybrids catalyze the reduction of O_2, even at relatively low pH values.[102]

■ ASSOCIATED CONTENT

Supporting Information

Summary of the synthesis conditions, powder XRD patterns for the copper and zinc hydroxide-based hybrids, IR and UV spectra of all compounds, SEM study, thermal analysis, ac susceptibility measurements for copper hydroxide-based compounds, additional X- and Q-band EPR spectra, simulation parameters of EPR spectra. This material is available free of charge via the Internet at http://pubs.acs.org.

■ AUTHOR INFORMATION

Corresponding Author

*E-mail: n.parizel@unistra.fr (N.P.), rogez@unistra.fr (G.R.).

Author Contributions

The manuscript was written through contributions of all authors. All authors have given approval to the final version of the manuscript.

Notes

The authors declare no competing financial interest.

■ ACKNOWLEDGMENTS

The authors thank the CNRS, the Université de Strasbourg, and the Agence Nationale de la Recherche (ANR contracts nos. 06-JCJC-0008 (COORDHYB) and 2010-BLAN-913-01 (C-BLUE)). The European COST action MP1202 (HINT) and the International Centre for Frontier Research in Chemistry (FRC) are also gratefully acknowledged. R.B. thanks the Algerian Ministry for High Education and Research (Direction for Cooperation and Inter-Universities Exchanges) for a grant. S.E.-M. thanks the French Ministry for Education and Research for his PhD grant. The authors thank C. Leuvrey, D. Burger, and M. Bernard for technical assistance and Dr. B. Vileno for fruitful discussions.

■ REFERENCES

(1) *Functional Hybrid Materials*; Gómez-Romero, P., Sanchez, C., Eds.; Wiley-VCH: Weinheim, 2004.
(2) *Chem. Soc. Rev.* 2011, *40*, Themed Issue on Hybrid Materials.
(3) *J. Mater. Chem.* 2005, *15*, Themed Issue on Functional Hybrid Materials.
(4) Li, M.; Mann, S. *Angew. Chem., Int. Ed.* **2008**, *47*, 9476−9479.
(5) Train, C.; Gheorghe, R.; Krstic, V.; Chamoreau, L.-M.; Ovanesyan, N. S.; Rikken, G. L. J. A.; Gruselle, M.; Verdaguer, M. *Nat. Mater.* **2008**, *7*, 729−734.
(6) Ogawa, M.; Kuroda, K. *Chem. Rev.* **1995**, *95*, 399−438.
(7) Clemente-Leon, M.; Coronado, E.; Marti-Gastaldo, C.; Romero, F. M. *Chem. Soc. Rev.* **2011**, *40*, 473−497.
(8) Train, C.; Gruselle, M.; Verdaguer, M. *Chem. Soc. Rev.* **2011**, *40*, 3297−3312.
(9) Clément, R.; Léaustic, A. In *Magnetism: Molecules to Materials II. Molecule-Based Materials*; Miller, J. S., Drillon, M., Eds.; Wiley-VCH: Weinheim, 2001; pp 397−423
(10) Coronado, E.; Martí-Gastaldo, C.; Navarro-Moratalla, E. N.; Ribera, A.; Blundell, S. J.; Baker, P. J. *Nat. Chem.* **2010**, *2*, 1031−1036.
(11) Pardo, E.; Train, C.; Liu, H.; Chamoreau, L.-M.; Dkhil, B.; Boubekeur, K.; Lloret, F.; Nakatani, K.; Tokoro, H.; Ohkoshi, S.-I.; Verdaguer, M. *Angew. Chem., Int. Ed.* **2012**, *51*, 8356−8360.
(12) Lacroix, P. G.; Malfant, I.; Bénard, S.; Yu, P.; Rivière, E.; Nakatani, K. *Chem. Mater.* **2001**, *13*, 441−449.
(13) Nicole, L.; Rozes, L.; Sanchez, C. *Adv. Mater.* **2010**, *22*, 3208−3214.
(14) Sanchez, C.; Ribot, F. *New J. Chem.* **1994**, *18*, 1007−1047.
(15) Forster, P. M.; Tafoya, M. M.; Cheetham, A. K. *J. Phys. Chem. Solids* **2004**, *65*, 11−16.
(16) Rabu, P.; Drillon, M.; Awaga, K.; Fujita, W.; Sekine, T. In *Magnetism: Molecules to Materials II. Molecules-Based Materials*; Miller, J. S., Drillon, M., Eds.; Wiley-VCH: Weinheim, 2001; pp 357−395.
(17) Rogez, G.; Massobrio, C.; Rabu, P.; Drillon, M. *Chem. Soc. Rev.* **2011**, *40*, 1031−1058.
(18) Martí, A. A.; Colón, J. L. *Inorg. Chem.* **2003**, *42*, 2830−2832.
(19) Lang, K.; Bezdička, P.; Bourdelande, J. L.; Hernando, J.; Jirka, I.; Káfuňková, E.; Kovanda, F.; Kubát, P.; Mosinger, J.; Wagnerová, D. M. *Chem. Mater.* **2007**, *19*, 3822−3829.
(20) Odobel, F.; Massiot, D.; Harrison, B. S.; Schanze, K. S. *Langmuir* **2002**, *19*, 30−39.
(21) Giannelis, E. P.; Nocera, D. G.; Pinnavaia, T. J. *Inorg. Chem.* **1987**, *26*, 203−205.
(22) Clément, R. *J. Am. Chem. Soc.* **1981**, *103*, 6998−7000.
(23) Delahaye, E.; Eyele-Mezui, S.; Diop, M.; Leuvrey, C.; Rabu, P.; Rogez, G. *Dalton Trans.* **2010**, *39*, 10577−10580.
(24) Eyele-Mezui, S.; Delahaye, E.; Rogez, G.; Rabu, P. *Eur. J. Inorg. Chem.* **2012**, *2012*, 5225−5238.
(25) Abellán, G.; Busolo, F.; Coronado, E.; Martí-Gastaldo, C.; Ribera, A. *J. Phys. Chem. C* **2012**, *116*, 15756−15764.
(26) Coronado, E.; Galán-Mascarós, J.-R.; Gómez-García, C.-J.; Ensling, J.; Gütlich, P. *Chem.—Eur. J.* **2000**, *6*, 552−563.
(27) Floquet, S.; Salunke, S.; Boillot, M.-L.; Clément, R.; Varret, F.; Boukheddaden, K.; Rivière, E. *Chem. Mater.* **2002**, *14*, 4164−4171.
(28) Clemente-León, M.; Coronado, E.; López-Jordà, M.; Mínguez Espallargas, G.; Soriano-Portillo, A.; Waerenborgh, J. C. *Chem.—Eur. J.* **2010**, *16*, 2207−2219.
(29) Clemente-León, M.; Coronado, E.; López-Jordà, M.; Waerenborgh, J. C.; Desplanches, C.; Wang, H.; Létard, J.-F.; Hauser, A.; Tissot, A. *J. Am. Chem. Soc.* **2013**, *135*, 8655−8667.
(30) Delahaye, E.; Eyele-Mezui, S.; Diop, M.; Leuvrey, C.; Foix, D.; Gonbeau, D.; Rabu, P.; Rogez, G. *Eur. J. Inorg. Chem.* **2012**, 2731−2740.
(31) Lever, A. B. P. In *Advances in Inorganic Chemistry and Radiochemistry*; Emeleus, H. J., Sharpe, A. G., Eds.; Academic Press: New York, 1965; Vol. 7, pp 27−114.
(32) Stillman, M. J.; Nyokong, T. In *Phtalocyanines, Properties and Applications*; Leznoff, C. C., Lever, A. B. P., Eds.; VCH Publishers: New York, 1989.
(33) McKeown, N. B. *Phthalocyanine Materials*; Cambridge University Press: Cambridge, U.K., 1998.
(34) Koca, A. *Electrochem. Commun.* **2009**, *11*, 838−841.
(35) Iliev, V.; Ileva, A.; Bilyarska, L. *J. Mol. Cat. A* **1997**, *126*, 99.
(36) Kaliya, O. L.; Lukyanets, E. A.; Vorozhtsov, G. N. *J. Porph. Phthal.* **1999**, *3*, 592−610.
(37) Martinez-Diaz, M. V.; de la Torre, G.; Torres, T. *Chem. Commun.* **2010**, *46*, 7090−7108.
(38) Inabe, T.; Tajima, H. *Chem. Rev.* **2004**, *104*, 5503−5534.
(39) Marks, T. J. *Angew. Chem., Int. Ed. Engl.* **1990**, *29*, 857−879.
(40) Craciun, M. F.; Rogge, S.; den Boer, M. J. L.; Margadonna, S.; Prassides, K.; Iwasa, Y.; Morpurgo, A. F. *Adv. Mater.* **2006**, *18*, 320−324.
(41) Liu, M. O.; Tai, C.-H.; Sain, M.-Z.; Hu, A. T.; Chou, F.-I. *J. Photochem. Photobio. A: Chem.* **2004**, *165*, 131.

(42) Lukyanets, E. A. *J. Porph. Phthal.* **1999**, *3*, 424−432.
(43) Vijayanathan, V.; Venkatachalam, S.; Krishnamurthy, V. N. *Synth. Met.* **2000**, *114*, 273−278.
(44) Bedioui, F. *Coord. Chem. Rev.* **1995**, *144*, 39−68.
(45) Seelan, S.; Sinha, A. K.; Srinivas, D.; Sivasanker, S. *J. Mol. Cat. A* **2000**, *157*, 163−171.
(46) Balkus, K. J.; Gabrielov, A. G.; Bell, S. L.; Bedioui, F.; Roue, L.; Devynck, J. *Inorg. Chem.* **1994**, *33*, 67−72.
(47) Yahiro, H.; Kimoto, K.; Yamaura, H.; Komaguchi, K.; Lund, A. *Chem. Phys. Lett.* **2005**, *415*, 126−130.
(48) Carrado, K. A.; Forman, J. E.; Botto, R. E.; Winans, R. E. *Chem. Mater.* **1993**, *5*, 472−478.
(49) Nakagaki, S.; Castro, K. A. D. F.; Machado, G. S.; Halma, M.; Drechsel, S. M.; Wypych, F. *J. Braz. Chem. Soc.* **2006**, *17*, 1672−1678.
(50) Carrado, K. A.; Winans, R. E. *Chem. Mater.* **1990**, *2*, 328−335.
(51) Rusling, J. F.; Ahmadi, M. F.; Hu, N. *Langmuir* **1992**, *8*, 2455−2460.
(52) Kafunkova, E.; Taviot-Guého, C.; Bezdicka, P.; Klementova, M.; Kovar, P.; Kubat, P.; Mosinger, J.; Pospisil, M.; Lang, K. *Chem. Mater.* **2010**, *22*, 2481−2490.
(53) Abellán, G.; Coronado, E.; Gómez-García, C. J.; Martí-Gastaldo, C.; Ribera, A. *Polyhedron* **2013**, *52*, 216−221.
(54) Ukrainczyk, L.; Chibwe, M.; Pinnavaia, T. J.; Boyd, S. A. *J. Phys. Chem.* **1994**, *98*, 2668−2676.
(55) Elena Pérez-Bernal, M.; Ruano-Casero, R.; Pinnavaia, T. *Cat. Lett.* **1991**, *11*, 55−61.
(56) Barbosa, C. A. S.; Ferreira, A.-M. D. C.; Constantino, V. R. L.; Coelho, A. C. V. *J. Incl. Phenom. Macro. Chem.* **2002**, *42*, 15−23.
(57) Park, I. Y.; Kuroda, K.; Kato, C. *Chem. Lett.* **1989**, 2057−2058.
(58) Hayashi, H.; Hudson, M. J. *J. Mater. Chem.* **1995**, *5*, 781−783.
(59) Coronado, E.; Martí-Gastaldo, C.; Navarro-Moratalla, E.; Ribera, A.; Tatay, S. *Inorg. Chem.* **2013**, *52*, 6214−6222.
(60) Ma, R.; Sasaki, T. *Adv. Mater.* **2010**, *22*, 5082−5104.
(61) Demel, J.; Pleštil, J.; Bezdička, P.; Janda, P.; Klementová, M.; Lang, K. *J. Colloid Interface Sci.* **2011**, *360*, 532−539.
(62) Schneiderová, B.; Demel, J.; Pleštil, J.; Janda, P.; Bohuslav, J.; Ihiawakrim, D.; Ersen, O.; Rogez, G.; Lang, K. *J. Mater. Chem. A* **2013**, *1*, 11429−11437.
(63) Laget, V.; Hornick, C.; Rabu, P.; Drillon, M.; Turek, P.; Ziessel, R. *Adv. Mater.* **1998**, *10*, 1024−1028.
(64) Shimizu, H.; Okubo, M.; Nakamoto, A.; Enomoto, M.; Kojima, N. *Inorg. Chem.* **2006**, *45*, 10240−10247.
(65) Laget, V.; Hornick, C.; Rabu, P.; Drillon, M.; Ziessel, R. *Coord. Chem. Rev.* **1998**, *178*−*180*, 1533−1553.
(66) Laget, V. Ph.D. Thesis, Université Louis Pasteur, Strasbourg, France, 1998.
(67) Laget, V.; Hornick, C.; Rabu, P.; Drillon, M. *J. Mater. Chem.* **1999**, *9*, 169−174.
(68) Demel, J.; Pleštil, J.; Bezdička, P.; Janda, P.; Klementová, M.; Lang, K. *J. Phys. Chem. C* **2011**, *115*, 24702−24706.
(69) Weber, J. H.; Busch, D. H. *Inorg. Chem.* **1965**, *4*, 469−471.
(70) Stoll, S.; Schweiger, A. *J. Magn. Reson.* **2006**, *178*, 42−55.
(71) Rueff, J.-M.; Nierengarten, J.-F.; Gilliot, P.; Demessence, A.; Crégut, O.; Drillon, M.; Rabu, P. *Chem. Mater.* **2004**, *16*, 2933−2937.
(72) Demessence, A.; Rogez, G.; Rabu, P. *Chem. Mater.* **2006**, *18*, 3005−3015.
(73) Delahaye, E.; Eyele-Mezui, S.; Bardeau, J.-F.; Leuvrey, C.; Mager, L.; Rabu, P.; Rogez, G. *J. Mater. Chem.* **2009**, *19*, 6106−6115.
(74) Yamanaka, S.; Sako, T.; Seki, K.; Hattori, M. *Solid State Ionics* **1992**, *53*−*56*, 527−533.
(75) Clearfield, A.; Tindwa, R. M. *J. Inorg. Nucl. Chem.* **1979**, *41*, 871−878.
(76) Pillet, S.; Souhassou, M.; Lecomte, C.; Rabu, P.; Drillon, M.; Massobrio, C. *Phys Rev. B* **2006**, *73*, 115116.
(77) Linder, G. G.; Atanasov, M.; Pebler, J. *J. Solid State Chem.* **1995**, *116*, 1−7.
(78) Masciocchi, N.; Corradi, E.; Sironi, A.; Moretti, G.; Minelli, G.; Porta, P. *J. Solid State Chem.* **1997**, *131*, 252−262.
(79) Villamil, R. F. V.; Corio, P.; Rubim, J. C.; Agostinho, S. M. L. *J. Electroanal. Chem.* **1999**, *472*, 112−119.
(80) Eyele-Mezui, S.; Delahaye, E.; Rabu, P.; Rogez G. manuscript in preparation.
(81) Fujita, W.; Awaga, K.; Yokoyama, T. *Inorg. Chem.* **1997**, *36*, 196−199.
(82) Laget, V.; Rabu, P.; Hornick, C.; Romero, F. M.; Ziessel, R.; Turek, P.; Drillon, M. *Mol. Cryst. Liq. Cryst.* **1997**, *305*, 291.
(83) Stählin, W.; Oswald, H. R. *Acta Cryst. Sect. B* **1970**, *26*, 860−863.
(84) Ma, R.; Liu, Z.; Takada, K.; Fukuda, K.; Ebina, Y.; Bando, Y.; Sasaki, T. *Inorg. Chem.* **2006**, *45*, 3964−3969.
(85) Neilson, J. R.; Morse, D. E.; Melot, B. C.; Shoemaker, D. P.; Kurzman, J. A.; Seshadri, R. *Phys Rev. B* **2011**, *83*, 094418.
(86) Neilson, J. R.; Schwenzer, B.; Seshadri, R.; Morse, D. E. *Inorg. Chem.* **2009**, *48*, 11017.
(87) Bauer, C.; Jacques, P.; Kalt, A. *Chem. Phys. Lett.* **1999**, *307*, 397−406.
(88) Taibi, M.; Ammar, S.; Jouini, N.; Fiévet, F.; Molinié, P.; Drillon, M. *J. Mater. Chem.* **2002**, *12*, 3238−3244.
(89) Park, S.-H.; Lee, C. E. *J. Phys. Chem. B* **2005**, *109*, 1118−1124.
(90) Kurmoo, M.; Day, P.; Derory, A.; Estournès, C.; Poinsot, R.; Stead, M. J.; Kepert, C. J. *J. Solid State Chem.* **1999**, *145*, 452−459.
(91) Alagna, L.; Capobianchi, A.; Casaletto, M. P.; Mattogno, G.; Paoletti, A. M.; Pennesi, G.; Rossi, G. *J. Mater. Chem.* **2001**, *11*, 1928−1935.
(92) Sharp, J. H.; Lardon, M. *J. Phys. Chem.* **1968**, *72*, 3230−3235.
(93) Sharp, J. H.; Abkowitz, M. *J. Phys. Chem.* **1973**, *77*, 477−481.
(94) Lever, A. B. P. *Inorganic Electronic Spectroscopy*, 2nd ed.; Elsevier: Amsterdam, 1984.
(95) Louër, M.; Louër, D.; Grandjean, D. *Acta Crystallogr.* **1973**, *B29*, 1696−1703.
(96) Panissod, P.; Drillon, M. In *Magnetism: Molecules to Materials IV*; Miller, J. S., Drillon, M., Eds.; Wiley-VCH: Weinheim, 2003; pp 233−270.
(97) Si, S.; Taubert, A.; Mantion, A.; Rogez, G.; Rabu, P. *Chem. Sci.* **2012**, *3*, 1945−1957.
(98) Carlin, R. L. *Magnetochemistry*; Springer-Verlag: Berlin, 1986.
(99) Laget, V.; Rouba, S.; Rabu, P.; Hornick, C.; Drillon, M. *J. Magn. Magn. Mater.* **1996**, *154*, L7.
(100) Drillon, M.; Panissod, P. *J. Magn. Magn. Mater.* **1998**, *188*, 93−99.
(101) Kurmoo, M. *Chem. Mater.* **1999**, *11*, 3370.
(102) Eyele-Mezui, S.; Bourzami, R.; Higy, C.; Turek, P.; Parizel, N.; Rabu, P.; Mousty, C.; Rogez, G. manuscript in preparation.
(103) Kalkan, A.; Güner, S.; Bayır, Z. A. *Dyes Pigm.* **2007**, *74*, 636−641.
(104) André, J.-J.; Bernard, M.; Piechocki, C.; Simon, J. *J. Phys. Chem.* **1986**, *90*, 1327−1330.
(105) Güner, S.; Şener, M. K.; Dinçer, H.; Köseoğlu, Y.; Kazan, S.; Koçak, M. B. *J. Magn. Magn. Mater.* **2006**, *300*, e530−e533.
(106) Neiman, R.; Kivelson, D. *J. Chem. Phys.* **1961**, *35*, 162−164.
(107) Gédéon, A.; Fraissard, J. *Colloids Surf., A* **1999**, *158*, 201−206.
(108) Marts, A. R.; Greer, S. M.; Whitehead, D. R.; Woodruff, T. M.; Breece, R. M.; Shim, S. W.; Oseback, S. N.; Papish, E. T.; Jacobsen, F. E.; Cohen, S. M.; Tierney, D. L. *Appl. Magn. Reson.* **2011**, *40*, 501−511.
(109) Bennett, B.; Holz, R. C. *J. Am. Chem. Soc.* **1997**, *119*, 1923−1933.
(110) Bennett, B.; Holz, R. C. *Biochemistry* **1997**, *36*, 9837−9846.
(111) Rollmann, L. D.; Iwamoto, R. T. *J. Am. Chem. Soc.* **1968**, *90*, 1455−1463.
(112) Finazzo, C.; Calle, C.; Stoll, S.; Van Doorslaer, S.; Schweiger, A. *Phys. Chem. Chem. Phys.* **2006**, *8*, 1942−1953.
(113) Moons, H.; Łapok, Ł.; Loas, A.; Van Doorslaer, S.; Gorun, S. M. *Inorg. Chem.* **2010**, *49*, 8779−8789.
(114) Delahaye, E.; Diop, M.; Welter, R.; Boero, M.; Massobrio, C.; Rabu, P.; Rogez, G. *Eur. J. Inorg. Chem.* **2010**, 4450−4461.